Biological network design strategies: discovery through dynamic optimization

Bambang S. Adiwijaya,[ab] Paul I. Barton*[c] and Bruce Tidor*[abd]

Received 14th July 2006, Accepted 16th October 2006
First published as an Advance Article on the web 27th October 2006
DOI: 10.1039/b610090b

An important challenge in systems biology is the inherent complexity of biological network models, which complicates the task of relating network structure to function and of understanding the conceptual design principles by which a given network operates. Here we investigate an approach to analyze the relationship between a network structure and its function using the framework of optimization. A common feature found in a variety of biochemical networks involves the opposition of a pair of enzymatic chemical modification reactions such as phosphorylation–dephosphorylation or methylation–demethylation. The modification pair frequently adjusts biochemical properties of its target, such as activating and deactivating function. We applied optimization methodology to study a reversible modification network unit commonly found in signal transduction systems, and we explored the use of this methodology to discover design principles. The results demonstrate that different sets of rate constants used to parameterize the same network topology represent different compromises made in the resulting network operating characteristics. Moreover, the same topology can be used to encode different strategies for achieving performance goals. The ability to adopt multiple strategies may lead to significantly improved performance across a range of conditions through rate modulation or evolutionary processes. The optimization framework explored here is a practical approach to support the discovery of design principles in biological networks.

Introduction

The development of quantitative models describing biological networks for a number of interesting systems is being undertaken.[1–23] These models aim to capture the underlying structure, dynamics, and detailed mechanisms of their experimental counterparts in a manner that recapitulates known behaviors, provides a means for understanding that behavior, and also predicts previously unmeasured or new behavior. The detail, accuracy, and number of systems for which models are available are all expected to grow for the foreseeable future. These models may potentially be used to generate hypotheses, understand design principles, create synthetic components, and produce effective therapeutic strategies. An important challenge is the inherent complexity of biological network models, which complicates the task of relating network structure to function and of understanding the conceptual design principles by which a given network operates.

[a]*Computer Science and Artificial Intelligence Laboratory, Massachusetts Institute of Technology, Cambridge, Massachusetts 02139-4307, USA*
[b]*Biological Engineering Division, Massachusetts Institute of Technology, Cambridge, Massachusetts 02139-4307, USA*
[c]*Department of Chemical Engineering, Massachusetts Institute of Technology, Cambridge, Massachusetts 02139-4307, USA. E-mail: pib@mit.edu*
[d]*Department of Electrical Engineering and Computer Science, Massachusetts Institute of Technology, Cambridge, Massachusetts 02139-4307, USA. E-mail: tidor@mit.edu; Fax: +1 (617) 252-1816; Tel: +1 (617) 253-7258*

Here we investigate one class of approaches for analyzing the relationship between network structure and functional behavior. We are concerned with dynamic properties, which may be particularly important for biological systems, although the same framework can address questions of steady-state behavior, which are generally simpler.

The overall approach involves applying optimization techniques to identify the best combinations of model parameter values to achieve canonical functional characteristics. In this manner, we study the relationship between model parameters (such as rate constants) and function. This complements, but differs fundamentally from, approaches in which systematic variation is applied to the parameters and the resultant change to behavior is monitored (sensitivity analysis and other variational approaches).[9,24–27] Here, essentially by manipulating the desired functional behavior (generally properties of the network output) and by monitoring the resultant required parameter values—*i.e.*, the inverse of more standard variational approaches—we can learn about the relationship between function and parameterization and may be in a position to discover new design principles. This approach works synergistically with variational analysis, which we then apply to dissect the roles of individual parameters.

The fundamental network unit examined here consists of the enzyme catalyzed chemical modification of a protein molecule and the reverse reaction catalyzed by a different enzyme. This basic unit is found repeatedly in multiple configurations throughout a wide variety of biological pathways, including methylation–demethylation reactions integral to bacterial chemotaxis[28] and phosphorylation–dephosphorylation

reactions of MAP kinase signaling cascades,[29] as just two specific examples of a very general motif. Here the generic nature of network architecture constructed from this basic unit will be emphasized by the use of general nomenclature and symbols, but the examples are motivated by current models of MAP kinase signaling cascades; model details, including canonical parameter values, were taken from that class of networks.

Fig. 1 illustrates the network topologies examined here. The fundamental unit involves the modification of protein A by enzyme F (for Forward modification) to give activated protein A'; protein A' is also unmodified by enzyme R (Reverse modification) to give protein A (Fig. 1a). For many applications it is useful to consider the activity of F as network input and the activity of A' as network output, although A and R activity are also important and will be treated as secondary inputs here. The enzymatic forward and reverse modification mechanisms were each treated as a single-substrate Michaelis–Menten reaction (Fig. 1b) with a coupled ODE model, as is typically done in many models of biological signal transduction; this is an approximation because it neglects the source and sink (such as binding of ATP and release of ADP, as well as any intervening chemistry) for the modification reactions, but when properly parameterized can be quite accurate for the case of ATP concentration significantly in excess of its effective dissociation constant (Fig. 1b–d). This fundamental network unit can be coupled to copies of itself (or to other units) to create a variety of topologies such as the two-step modification typical of an individual layer of MAP kinase pathways (Fig. 1e), in which the output of the first unit acts as a secondary input (substrate) to the next unit, which then produces the final output.[10] In this example, the same input, F, is applied in parallel to both units, as is R. Another topology studied here is the simplified two-layer network shown in Fig. 1f, in which the output of the first unit serves as the input (forward modification enzyme) to the second, which is a form of series connection. Repeating the fundamental unit six times with appropriate interconnections reproduces common models of MAP kinase cascades that use no scaffolding interactions (Fig. 1g).

The optimization approach taken here utilizes a simulation model for the biological network, a search space, and one or more objective functions. Additionally, sets of constraints are employed in some applications. For the simulation, we used

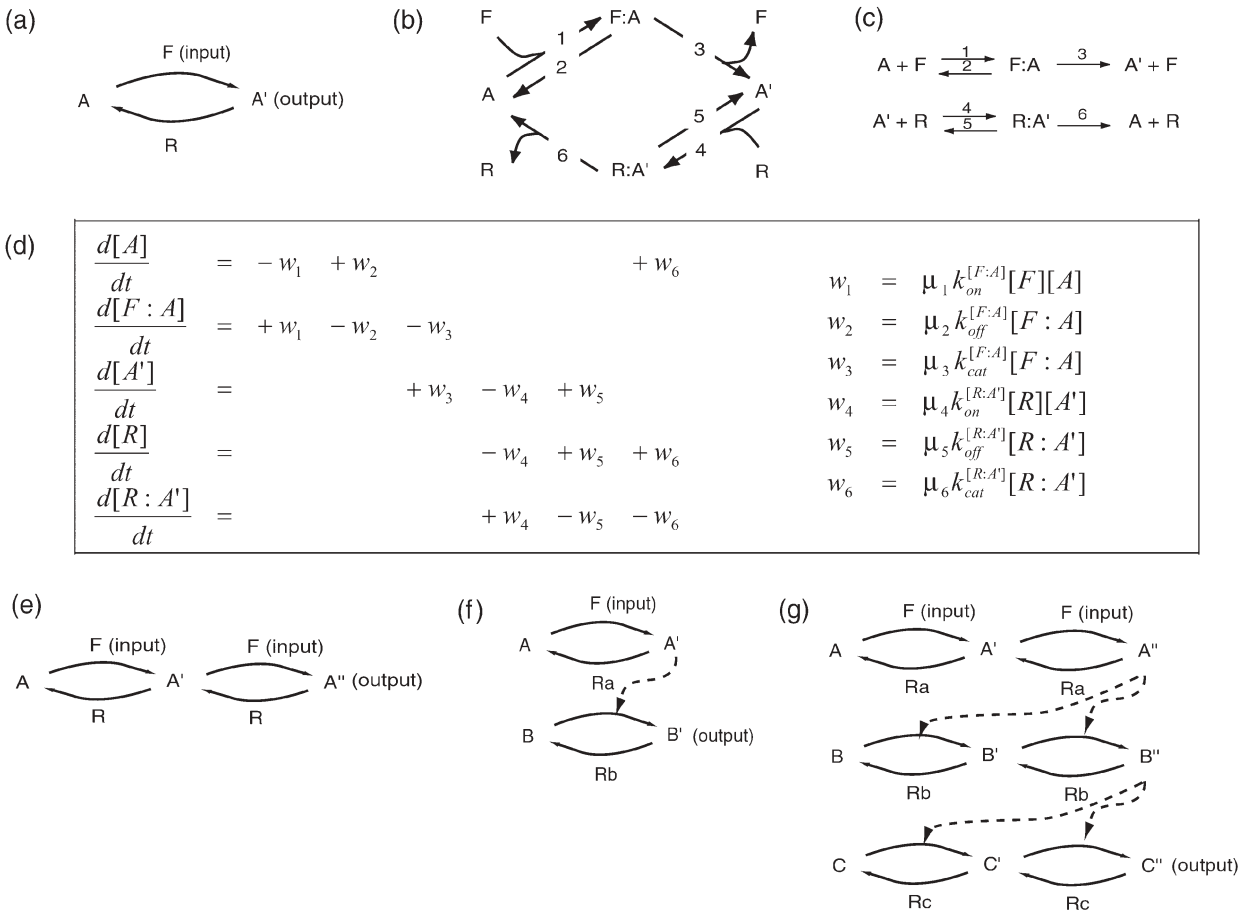

Fig. 1 Alternative representations of the fundamental enzymatic modification and reverse modification reactions. (a) Schematic of a one-step modification and reverse modification reaction network; (b) alternative representation of the network given in (a), with emphasis on conservation of A; (c) chemical reaction network representation of the network given in (a); (d) mass-action dynamic equations of the network given in (a); (e) schematic of a two-step modification and reverse modification network; (f) schematic of a two-layer cascade with one-step modification and reverse modification in each layer; (g) schematic of a three-layer cascade network with two-step modification and reverse modification in each layer, which represents a common model of scaffold-free MAP kinase cascades.

mass-action kinetic models with state variables corresponding to biomolecule concentrations, parameters corresponding to kinetic rate constants, and initial conditions defining total biomolecule concentrations and their distribution at the start of the simulation. The models used simulate fundamental steps of signal transduction cascades in biological systems. Mass–action kinetic models have been popular and successful for simulating biological networks, although there are certain limitations and approximations inherent in their use; some of these limitations can be avoided with other modeling methods, such as stochastic approaches.[3,30] The search space corresponded to ranges for the individual parameters that were considered during the optimization. Here each rate constant was varied continuously about its canonical value through a range from three orders of magnitude smaller to three orders of magnitude larger ($k_i = \mu_i k_{i,0}$ for $\mu_i \in [10^{-3},10^{3}]$). We are also investigating variation of the network topology in addition to parameterization. Here, the network topology was varied manually; systematic variation of topology and parameterization may be formulated as a simultaneous optimization of discrete and continuous variables, but is beyond the scope of this paper. The objective function describes the desired functional behavior of the network to be minimized or maximized. Here we have focused on single-input-single-output networks and, for illustrative purposes, we have examined the objectives of response-time and signal amplification. These functional characteristics correspond to measures of how quickly and accurately changes in output follow changes to the input signal.

To examine the consequences of competing effects, we carried out optimization runs with one function as the objective function and another enforced as a constraint. In particular, by enforcing a constraint on signal amplification, we have clarified how different strategies for minimizing response-time are encoded in a single network topology. Interestingly, the strategy that is more optimal depends on the desired level of signal amplification. That is, the results suggest that a fixed topology network consisting of linked enzyme-catalyzed reactions can adopt multiple strategies through varying only rate parameters over a relatively modest range. The ability to adopt multiple strategies may lead to significantly improved performance under changing conditions on evolutionarily accessible time-scales. Also, the use of chemical modification or binding modulators can customize the same generic network to operate with different strategies under different conditions.

Methods

Models

Canonical parameter values were obtained from the work of Huang and Ferrell[10] (Table 1). Here wide ranges of rate constant parameter values were systematically examined spanning three orders of magnitude to either side of the canonical value ($k_i = \mu_i k_{0,i}$ for $\mu_i \in [10^{-3},10^{3}]$). For the networks in Fig. 1a, e, and f, all six or twelve parameters were varied during optimization; for the full MAP kinase cascade of Fig. 1g, we limited the size of the optimization problem by varying only the association rate constants between an enzyme and its substrates both for modification and reverse modification steps, for a total of twelve variables.

Table 1 Canonical parameter values in a unit network of one-step activation–deactivation reactions

Parameter	Canonical value	References
$k_{on}^{[F:A]}$	0.1 μM^{-1} s^{-1}	7, 44
$k_{off}^{[F:A]}$	0.033 s^{-1}	7, 44
$k_{cat}^{[F:A]}$	16 s^{-1}	7, 44
$k_{on}^{[R:A']}$	5 μM^{-1} s^{-1}	10
$k_{off}^{[R:A']}$	0.5 s^{-1}	10
$k_{cat}^{[R:A']}$	0.3 s^{-1}	10
$[F]_0$	20 μM	7
$[A]_0$	34 μM	7
$[R]_0$	16 μM	7
$[F:A]_0$	0 μM	Problem definition
$[A']_0$	0 μM	Problem definition
$[R:A']_0$	0 μM	Problem definition

Optimization functions

Parameter values were computed to optimize functional characteristics of the network topologies examined. Two target functions were used individually in the calculations, which are defined by the following equations:

$$f_{response} = f_{rise} + f_{decay} = \int_0^{T_\delta} \left(\frac{[O]-[O]_{ss}}{[O]_{ss}} \right)^2 dt + \int_{T_\delta}^{T_f} \left(\frac{[O]}{[O]_{ss}} \right)^2 dt \quad (1)$$

$$[O]_{ss} = [O](T_\delta) \quad (2)$$

where $[O](t)$ is the activity (equivalent to concentration here) of the network output (in Fig. 1), which is $[A']$ for parts a–d, $[A'']$ for part e, $[B']$ for part f, and $[C'']$ for part g; $[O]_{ss}$ is the steady-state value of the output while a constant input is applied. Each objective function was studied in the context of the response to a square wave input pulse of width T_δ and amplitude F_0 (see Fig. 2). The response-time objective, $f_{response}$, measures how quickly and accurately step changes to network input are reflected in the output. T_f is a time sufficiently long that the network has returned to its unmodified state. The value of the objective evaluated for a given network with a given input pulse is zero if the output tracks the input perfectly (pure amplification) and accumulates an increasingly positive value for increasing discrepancies. Normalization by the steady-state output achieved with constant input provides a comparable objective for networks of varying attenuation. The response-time objective is the sum of two parts, f_{rise} that quantifies the fidelity of the network in replicating the *on* or *rise* portion, and f_{decay} that is defined similarly for the *off* or *decay* portion. Eqn (2) was used to enforce a constraint on the magnitude of signal output.

Simulation and optimization

Simulations were performed with the DSL48S program[31] within the ABACUSS package (version 2).[32] The problem formulation for the work reported here involves differential algebraic equations (DAEs) that are both stiff and sparse. The

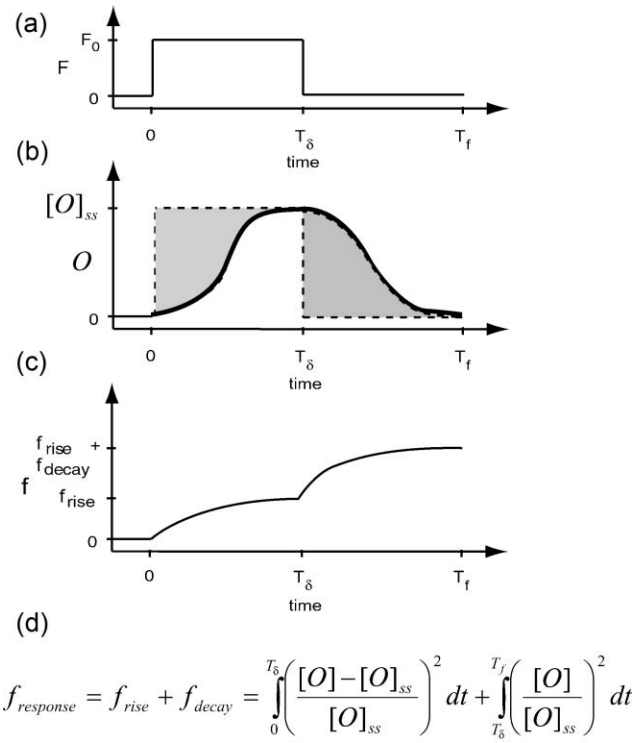

$$f_{response} = f_{rise} + f_{decay} = \int_0^{T_\delta} \left(\frac{[O]-[O]_{ss}}{[O]_{ss}} \right)^2 dt + \int_{T_\delta}^{T_f} \left(\frac{[O]}{[O]_{ss}} \right)^2 dt$$

Fig. 2 The definition of the response-time objective (f_{response}) and the output amplitude ($[O]_{\text{ss}}$) constraint. (a) A square wave input trajectory was used to stimulate each network; (b) an output trajectory after stimulation; rise- and decay-time objectives are related to the earlier and later grey regions, respectively; (c) the rise-, decay-, and response-time objective trajectories after stimulation; (d) the mathematical definition of rise, decay, and response-time objectives.

differential equations are fundamental to the kinetic chemical model of the biochemistry; the algebraic equations enter through a flux model formulation, in which the differential equations are written in terms of the fluxes along each reaction, and these fluxes are in turn equal to simple algebraic rate laws (see Fig. 1d). While perhaps not necessary for problems of this small size, this approach is more efficient because the substitution reduces the need for repeat computations and can produce an improved sparsity pattern.[33] A stiff solver is necessary for efficient computation of at least some simulations made because parameter ranges spanning six orders of magnitude were involved, creating the opportunity for vastly different time-scales within one simulation. The system of equations is sparse because the time derivative of each activity or concentration (state variables) depends on only a small number of the other state variables. The DSL48S program uses a staggered corrector method[31] for efficient sensitivity calculation, a large-scale sparse linear algebra package MA48[34] to make efficient use of sparsity, and a backward difference formula (BDF)[35] to deal with stiffness. The solution for the set of rate constant multiplier values (μ_i variables) that minimizes the objective function for a given differential equation model, set of initial conditions, and set of constraints is solved with the control parameterization algorithm,[36] where the system dynamics (including objective function and constraints, as well as their derivatives with respect to the optimization variables [sensitivities]) are solved for given values for the optimization variables, and this information is used iteratively to carry out nonlinear optimization in the space of the optimization variables to minimize the objective function subject to the constraints. Ideally, the optimization problem with embedded dynamics should be solved with a deterministic global optimization algorithm. We are working on methodology to achieve that goal.[37] For the current work, local optimization of variables was carried out from a large number of random starting points (multi start). The local optimization was carried out with the nonlinear programming (NLP) solver NPSOL, which implements a successive quadratic programming algorithm.[38] NPSOL terminates each local optimization when a Karush–Kuhn–Tucker (KKT)[39,40] point is reached, to within a numerical tolerance of 10^{-6} s. It should be noted that in an unconstrained feasible set, a local minimum is a point with zero gradient. For the work reported here, optimization was carried out in a bounded set of optimization variables consisting of the logarithms of the rate constant multipliers (bounded by -3 and $+3$). Values of $T_\delta = 10$ s and $T_f = 110$ s were used. Simulations were initiated from an equilibrated point in the absence of F (Table 1) at time $t = 0$. Local optimization from a large number of random starting points was used; the best optimum was taken as the global optimum. As a check on convergence, for the six-variable problem, when ten times as many runs were performed, no new lowest local optimum was observed. Problems with six (twelve) parameter variables were repeated from 1000 (20 000) randomly generated starting points uniformly distributed on the logarithmic scale, and the lowest local optimum was observed 10 (3–5) times. Typically each optimization run in a multi-start set required 3 s (75 s) for a six- (twelve-) variable problem using a single 2.8 GHz Intel Pentium III Xeon processor. The six-variable problem corresponds to the one-step network (Fig. 1a), and the twelve-parameter problem corresponds to the two-step, the two-layer, and the kinase cascade networks (Fig. 1e, f, and g).

Results and discussion

The fundamental network unit consisting of a pair of Michaelis–Menten enzymatic forward and reverse modification reactions (Fig. 1a–d) was studied using optimization methodology. The response-time objective function f_{response} was minimized while all six rate constant multipliers were permitted to vary subject to a series of constraints applied to the steady-state amplitude of the network output ($[O]_{\text{ss}}$; 10^{-6} μM $\leqslant [O]_{\text{ss}} \leqslant$ 34 μM; Fig. 2). Total concentrations of $[A]_0$ and $[R]_0$ were fixed (Table 1) and the same input square pulse of $[F]$ (pulse height of $[F]_0 = 20$ μM; pulse width of $T_\delta = 10$ s) was applied for each optimization. The results are shown in Fig. 3. The characteristics of the trade-off between f_{response} and $[O]_{\text{ss}}$, along with representative global optimal networks for each value of the $[O]_{\text{ss}}$ constraint are illustrated schematically in the figure. In each optimal network, a red (green) reaction arrow indicates that the corresponding rate constant was driven toward its minimum (maximum) value through optimization; a blue reaction arrow indicates that an

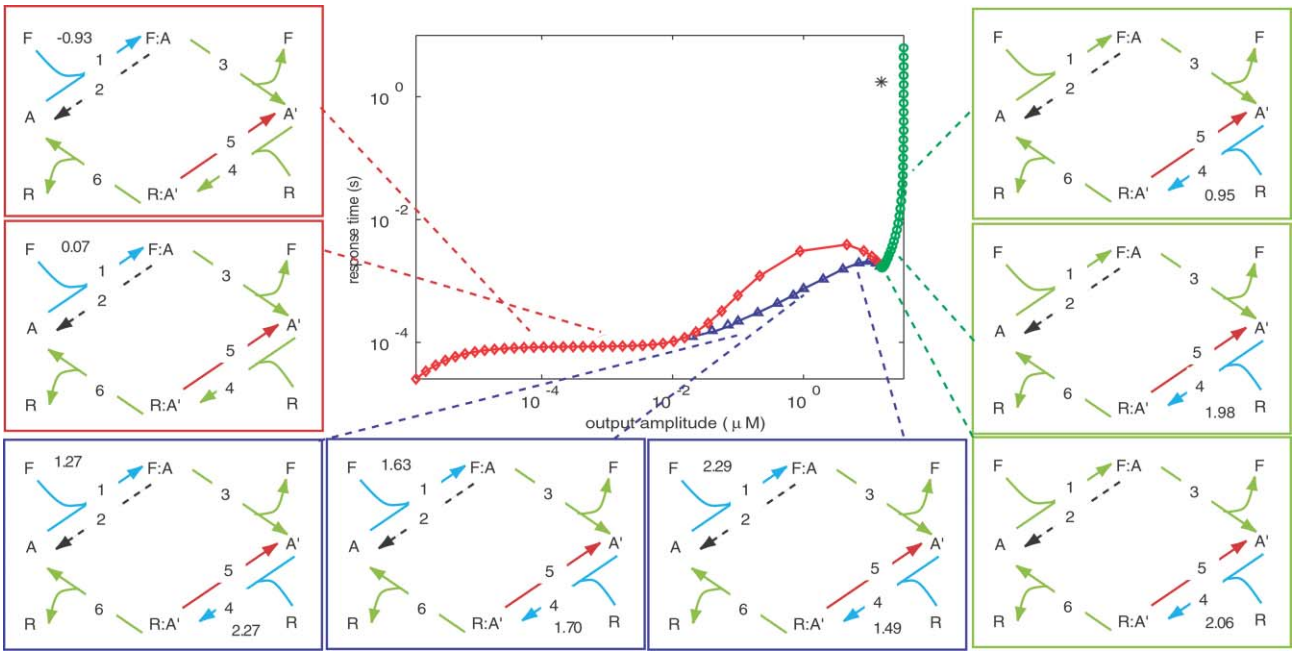

Fig. 3 Trade-off curve of response-time and output amplitude objectives, along with representative optimal networks. Color scheme for reaction arrows: green, the rate is maximized to the upper bound; red, the rate is minimized to the lower bound; blue, the rate is optimized to a value between both bounds (the optimal value of $\log_{10}(\mu_i)$ is indicated); black-dotted, the rate is insensitive in the regions explored. Asterisk, when network is parameterized with the canonical MAP kinase values obtained from ref. 10. Strategy one network examples are enclosed in a red box, strategy two in a blue box, and strategy three in a green box.

optimized rate constant was driven to an intermediate value; a black dashed arrow indicates that the system was insensitive to that rate parameter (*i.e.*, the objective changed by less than one percent for a six-order-of-magnitude variation of the corresponding rate constant).

Interestingly, the pattern of optimized rate constants found over the set of optima obtained with different amplitude constraints clustered into three distinct groups that can be thought of as strategies for achieving the minimum response-time objective. Strategy one, involving an intermediate value of μ_1 (the first forward reaction) and high value of μ_4 (the first reverse reaction), was optimal at low values of the output amplitude constraint; strategy three, involving a high value of μ_1 and an intermediate value of μ_4, was optimal for high amplitude constraint values; and strategy two, combining aspects of the other two optima, was optimal for intermediate amplitude constraint values. Other characteristics were common to all three strategies, including small values of μ_5, insensitivity to μ_2, and maximal values of other rate constants.

To determine the advantages attained by a network that optimizes to a particular strategy, we repeated the optimization with the network locked artificially into each of the three observed strategies. This was achieved by applying the appropriate constraints during the optimization that correspond to the desired strategy. For example, to lock into strategy one, μ_3, μ_4 and μ_6 were constrained to 10^3, and μ_5 was constrained to 10^{-3}. The resulting trade-off curves are also shown in different colors in Fig. 3 (red, blue, and green for strategies one, two, and three, respectively); they reveal that each strategy can only cover a limited range of amplitude constraints. Outside of that range, no set of rate constant values within the defined bounds and strategies can meet the constraints. Furthermore, in the region where strategies one and two overlap, we observed that the network produced a worse response-time objective when locked into strategy one than when it was allowed to adopt the more optimal strategy two, suggesting a disadvantage for a network committed to a single strategy.

To examine the search landscape encountered by the network, we systematically varied each of the six parameter variables, μ_1–μ_6, starting from an optimum corresponding to strategy one, two, or three, and examined the effect on the response-time and output amplitude objectives. For completeness, we also examined a base strategy with the four "progressive" reactions (μ_1,μ_3,μ_4,μ_6) being as fast as possible and the two "opposing" reactions (μ_2,μ_5) being as slow as possible (for which $f_{\text{response}} = 0.000577$ s and $[O]_{\text{ss}} = 15.4$ μM). Although this one-dimensional parametric variation covers only a small portion of the search space, it is useful to examine the related strategies observed above. The results, shown in Fig. 4, portray a sample of the search landscape that contains both nonconvex and insensitive regions. For example, for all of the strategies the effect of μ_1 on the response-time reveals two local optima (one at low and one at high μ_1 values), and an insensitive region near the low μ_1 value. In the absence of output constraints, our multi-start optimization procedure produced locally optimal solutions both at low and high values of μ_1 (data not shown). Moreover, the insensitive regions led to multiple local solutions (data not shown). It should be noted that in Fig. 4 the parametric variation caused the system to no longer satisfy the amplitude constraint, thus, although some parameter combinations appear more optimal than the

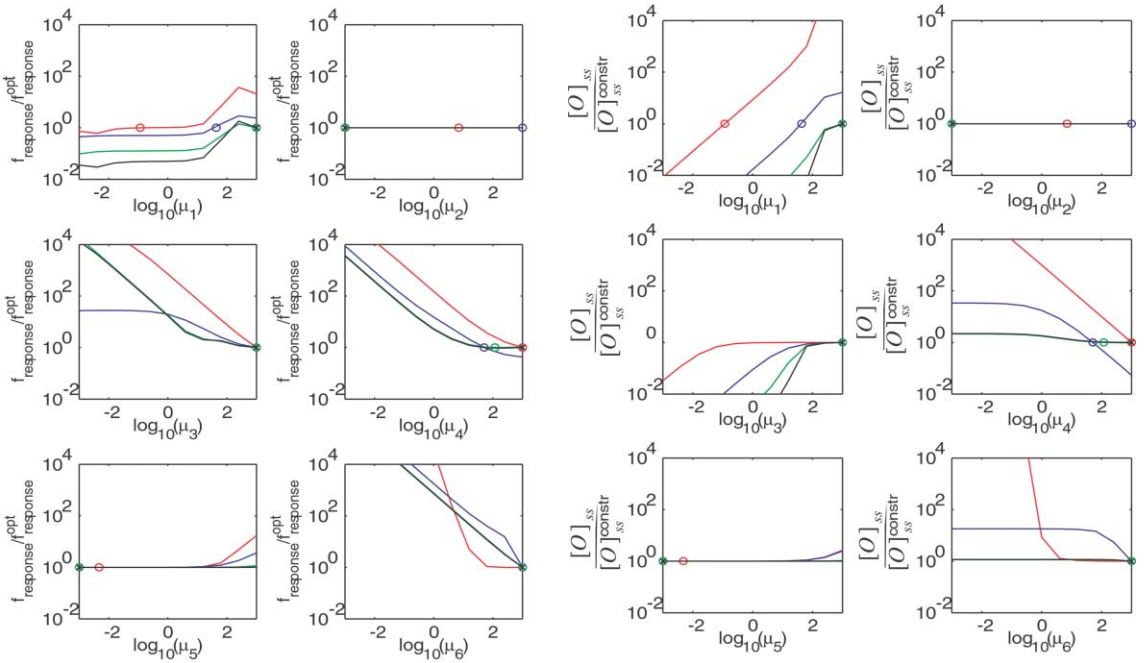

Fig. 4 One-dimensional parametric variation of response-time and amplitude objectives for four strategies. Legends: red, strategy one (with amplitude of 10^{-4} μM); blue, strategy two (with amplitude of 1 μM); green, strategy three (with amplitude of 20 μM); and black, the base strategy, with all "progressive" reactions maximized and all "opposing" reactions minimized. The objective values are normalized to the optimal values of each respective strategy. The symbols represent the unperturbed parameter values.

computed optimum, they are not, because they fail to satisfy the required constraint.

Interestingly, Fig. 4 also illustrates a striking range of variability among the various rate constants. The rate constants k_2 and k_5 have very little effect on f_{response} and $[O]_{\text{ss}}$ for all strategies. At the other extreme, k_3, k_4, and k_6 strongly affect f_{response}, with smaller rates generally leading to worse (slower) response-time objectives. Likewise, k_1 and k_3 have strong effects on $[O]_{\text{ss}}$ for all strategies, with slower rates producing smaller $[O]_{\text{ss}}$, but k_4 and k_6 show strong effects on $[O]_{\text{ss}}$ only for strategies one and two, with slower rates generally increasing $[O]_{\text{ss}}$. This figure illustrates some of the trade-offs inherent in moving between strategies. The strategy two f_{response} behavior for k_4 indicates the ability to reach a shorter response-time by increasing k_4 to its maximum value ($\mu_4 = 10^3$) and thus switching to strategy one; however, this change also decreases $[O]_{\text{ss}}$. This parallels the observations of Fig. 3 showing that strategy two is optimal for intermediate amplitudes and strategy one for low amplitudes, with a smaller value of the response-time objective.

A fundamental challenge of biological network modeling is to extract conceptual understanding of networks and the strategies that they adopt. Strategies are likely to be selected because of their desirable functional properties across a wide range of conditions and time-scales (including evolutionary time-scales), and it is unclear to what extent snapshots of biological networks are expected to behave optimally. Nevertheless, there is ample evidence to suggest that sufficient optimization has occurred so that much can be learned by studying biological systems from this perspective.[41,42] With this goal, we have undertaken to understand in more detail the conceptual basis for the strategies adopted here.

No general methodologies exist that are guaranteed to extract this type of understanding from biological network models, which are inherently nonlinear, but a number of tools have been applied to the problem.[4,5,24,25,43] Strategy one is particularly counterintuitive in that the first forward reaction, which is the first step in generating the output signal, is actually slowed to minimize response-time. Here we have adopted a combination of variational analysis and objective decomposition to study the mechanistic basis for strategy one.

Starting from the strategy one optimum with $[O]_{\text{ss}} = 1.0 \times 10^{-4}$ μM, the value of μ_1 was systematically varied across the range of $[10^{-3},10^3]$ with all other parameter variables fixed at their optimal values, as was done for the data in Fig. 4. The value of the response-time objective was monitored, as were the separate rise-time and decay-time objectives that comprise the response-time. The results, shown in Fig. 5b with logarithmic ordinate scale, demonstrate that the rise-time has two minima (one at low and the other at high μ_1 values), while the decay-time increases monotonically with increasing μ_1; the result is an overall response-time objective that also has two minima, one at low and another at high μ_1 values, with the former being a global minimum. Thus, in the neighborhood of this strategy one optimum, choosing a smaller μ_1 value produces faster rise- and decay-times, and consequently response-time, than maximizing μ_1 to its upper bound.

We compared the previous strategy one to strategy three with $[O]_{\text{ss}} = 15.9$ μM and where μ_1 was driven to its upper bound (Fig. 5f). In this strategy, μ_4 optimized to $10^{2.06}$, a value different from that of strategy one (10^3), and consequently, the

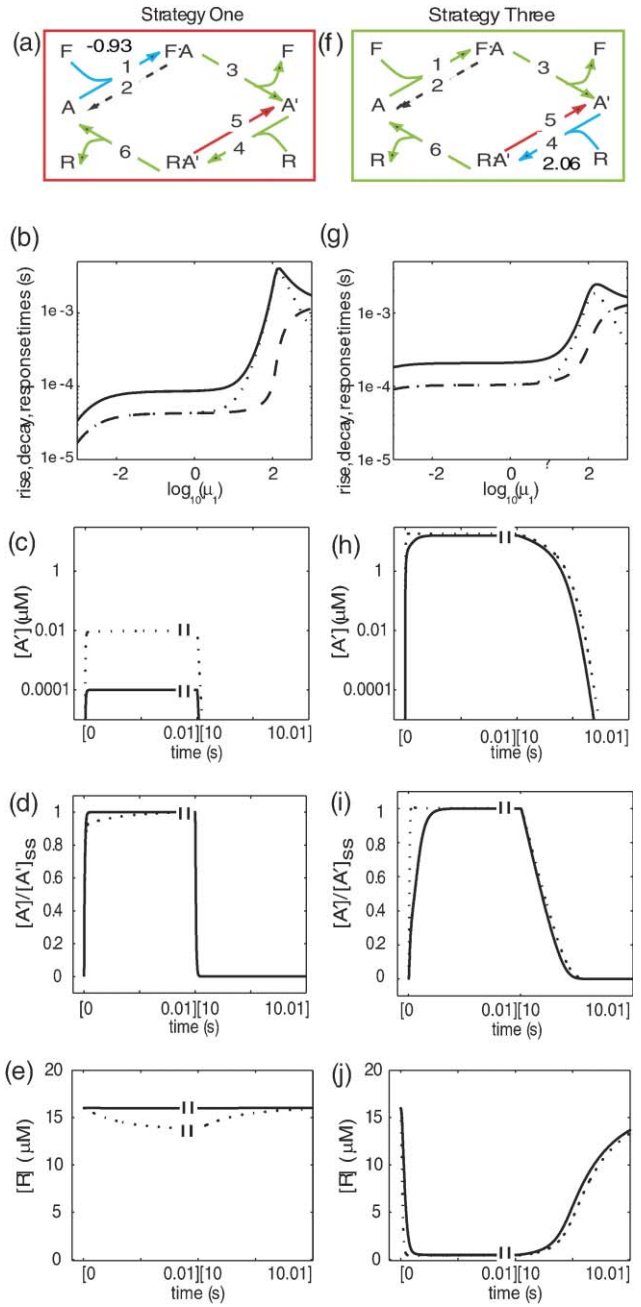

Fig. 5 Decomposition and variational analysis of optimal strategies. (a),(f), Response-time optimal networks; (b),(g), sensitivities of rise- (dotted line), decay- (dashed line), and response-time (solid line) objectives to rate constant multiplier μ_1; (c),(h), trajectory of $[A']$ for the corresponding strategy (solid line) and when μ_1 is increased by 100-fold (dotted line); (d),(i), similar to (c) and (h), but normalized by steady-state of A'; (e),(j), trajectory of R for the corresponding strategy (solid line) and when μ_1 is increased 10-fold (dotted line); (a–e), applied to strategy one; (f–j), applied to strategy three.

nearby search landscape may potentially differ between the two strategies. When we subjected strategy three to the same decomposition analysis, we discovered that the rise-, decay-, and response-time objectives were qualitatively similar to (but quantitatively different from; see Fig. 5g) the strategy one results: the rise- and response-times had minima at both low and high μ_1, while the decay-time monotonically increased with increasing μ_1. For this strategy, choosing a smaller μ_1 value also produced a smaller response-time solution, but this smaller μ_1 value was inferior to the one of strategy one.

We examined the trajectories of $[A']$ that are used to compute these objectives. The traces of $[A']$ for both strategies one and three are plotted (in solid lines) along with the trajectories obtained when the μ_1 was perturbed (in dotted lines) nearby its values of the two strategies in Fig. 5c and h, respectively. Each panel of the figure is composed of two tiles, the first covering the initial 0.01 s after the input was switched on and the second covering the initial 0.01 s after the 10 s input pulse was switched off. As these trajectories indicate, the transient is much shorter than 0.01 s, and this network is capable of very fast responses. These traces show an interesting difference between strategy one and strategy three—namely, for strategy one the $[A']$ rises sharply and levels off essentially instantly at the start of the initial 0.01 s window, but for strategy three $[A']$ rises to a higher value and "tails" into the steady-state value. The result is that strategy three has a longer (worse) response-time objective. The effect of increasing μ_1 in strategy one moves the steady state further away (10-fold) and increases the reaction velocity toward the new steady state. The former effect dominates the latter, as demonstrated by plotting $[A']$ normalized to its steady-state value, shown in Fig. 5d; the perturbed case has $[A']$ approaching its steady-state more slowly than the unperturbed case. For strategy three, the pattern of dominance switches; increasing μ_1 affects the initial velocity more than the steady state, and as a result a faster approach to steady state is observed, as shown in Fig. 5i.

Only one side of the same trade-off is observed for the decay portion of the objective. The traces for $[A']$ in Fig. 5c and h highlight the vast difference in the decay-time behavior between strategies one and three—almost instantaneous decay for strategy one and a substantially larger decay-time (about 0.001 s) for strategy three. Moreover, in both strategies, increasing μ_1 produces a somewhat worse decay-time objective although visually this is hardly observable in the normalized $[A']$ trajectories. The decay portion requires removing A' by reacting it with R, whose concentration trajectory is plotted in Fig. 5e and j. Interestingly, although the total amount of R in all forms is the same for both situations, at the end of the input pulse, $[R]$ is 15.98 μM for strategy one and 0.495 μM for strategy three. The larger pool of R for strategy one corresponds with the fast decay-time for that case. The small pool of R for strategy three is less than the amount of A' to be depleted and must be used catalytically. Increasing μ_1 has the effect of slightly reducing $[R]$ at the time the input pulse is turned off and leads to a somewhat worse decay-time.

We extended the optimization and analysis both to a two-step and to a two-layer network, whose reaction schemes are given in Fig. 1e and f, respectively. The former corresponds to modification and reverse modification enzymes that process their substrate twice; the latter corresponds to a cascade in which activation of substrate A to A' produces a new modification activity that acts on a second substrate, B; a pair of reverse modification enzymes, R_a and R_b, operate on A' and B', respectively. Optimization allowed all twelve parameters in either scheme to vary over six orders of magnitude

while minimizing the response-time objective subject to a constraint on the output amplitude. The optimization results are shown in Fig. 6. The data indicate that the two-step network adopts six strategies that we could identify (Fig. 6a), which is more than the three strategies observed for the one-step network. The two-step network contains one modification–reverse modification cycle that interconverts A and A', and a second cycle interconverting A' and A''. Interestingly, the optimization results indicate that some of the new strategies adopted by the two-step network correspond to combinations of the strategies described above for the one-step network, with the first cycle adopting strategy one and the second cycle adopting strategy three, for instance. Other strategies adopted by the two-step network are novel and do not appear to reflect a composite of the one-step results.

For the two-layer network, only three strategies were observed that displayed an optimal response-time objective for some amplitude constraint (Fig. 6b). Each strategy was a composition of the strategies observed for the one-step network. One of these combinations, strategy one for the first cycle and strategy three for the second, produced the optimal solution over nearly the entire range of amplitude constraints studied.

In general, one would expect that a network with more degrees of freedom would achieve better optima than one with fewer degrees of freedom, everything else being equal. The extra degrees of freedom should admit better solutions. Here the one-step network had six rate constant degrees of freedom, whereas the two-step and two-layer networks had twelve; yet the one-step network optima produced uniformly lower values of the minimized response-time objective for all values of the amplitude constraints. The additional degrees of freedom for the two-step and two-layer networks were counterbalanced by the extra network latency involved with a longer path from input to output. For the cases studied here, the latency delays dominated.

Finally, the same optimization and analysis framework was applied to a network consisting of two modification steps and a three-layer kinase cascade, whose scheme is shown in Fig. 1g. This corresponds to models commonly used for MAP kinase signaling cascades. Because of the much larger number of parameters in this model, for this initial study we optimized only the association rate constants, leaving all others at their canonical values, for a total of 12 variable parameters. When compared with the two-step and two-layer networks, the response-time objective values for this kinase cascade are slower (higher), in agreement with the trends observed for both the two-step and two-layer networks as compared with the one-step network. For example, the response-time for the kinase cascade ranges from 58–238 s (the range for the two-step network is 0.0003–0.002 s and for the two-layer network is 0.0002–0.004 s for the same amplitude range of 10^{-4}–10 μM). Interestingly, this kinase cascade is able to produce a more consistent range of objective values across amplitude constraints (roughly 4-fold) than that of the two-step and two-layer networks (7–20-fold). The cascade displays optimal strategies that include combinations of those observed for the one-step network (Fig. 7). In particular, in the bottom layer of the cascade, where the output is measured, the optimal strategy corresponding to an effective one for the two-step network is consistently used, with strategy two for the first cycle and strategy three for the second. Because not all rate parameters were varied here, these are the closest analogs to the observed strategies. Modulation of the amplitude while minimizing the response-time is achieved by varying rate parameters in the first and second layers.

In other work, Heinrich *et al.* have examined analytically solvable models of protein kinase signal transduction cascades.[23] That work is complementary to the work presented here in that it uses a simpler form of model that is more amendable to analytic solutions, with all the benefits of an analytic solution. Here we have focused on using computational methods to explore the parameter space and were able to use a somewhat more detailed model. Likewise, the use of optimization facilitated the isolation of ideal parameter values for achieving specific ends. The functions used to characterize signal response were somewhat different between the two works; the previous work focused on average signal time, duration, and effective amplitude, while in this work the focus was on the rapidity with which the output signal responded to

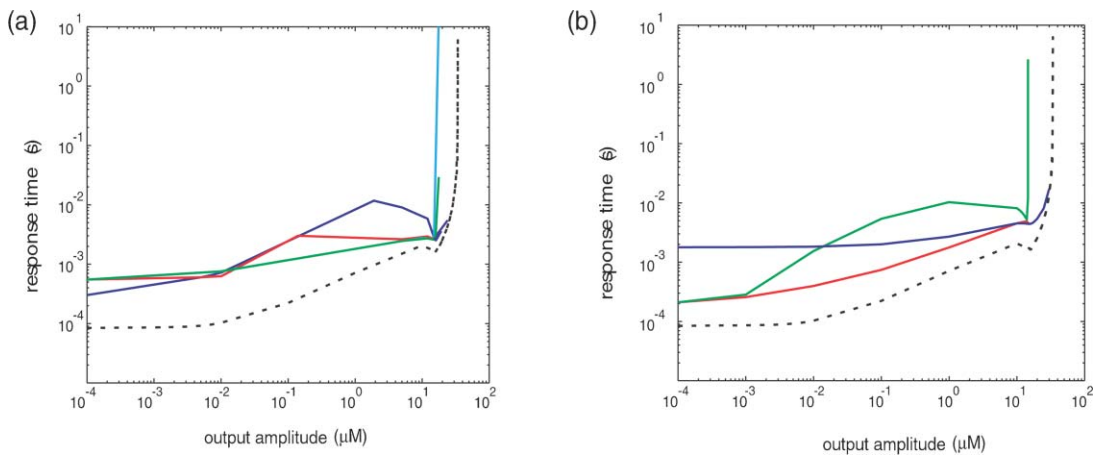

Fig. 6 Trade-off curve for response-time and output amplitude objectives for variant networks. (a) The two-step network given in Fig. 1e; (b) the two-layer network given in Fig. 1f. Legends: solid lines, multiple strategies in each network; dotted line, trade-off curve for one-step network.

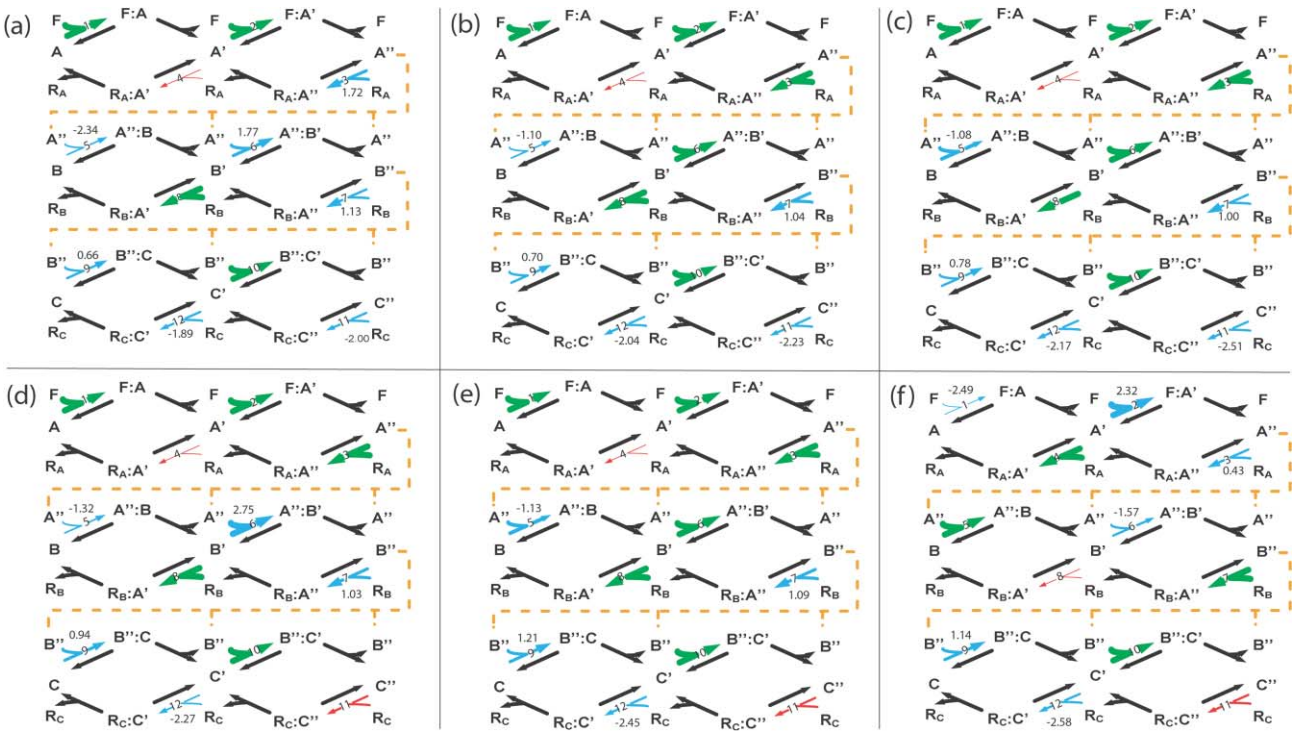

Fig. 7 The response-time optimal kinase cascade networks for multiple amplitude constraints. (a) For an amplitude of 10^{-4} μM; (b) for an amplitude of 10^{-3} μM; (c) for an amplitude of 10^{-2} μM; (d) for an amplitude of 10^{-1} μM; (e) for an amplitude of 1 μM; (f) for an amplitude of 10 μM;

changes in the input signal. In related work, Markevich *et al.* demonstrated that two-site MAP kinase phosphorylation and dephosphorylation cycles were capable of producing bistability.[21] In the context of the current study, for systems with multiple kinase and phosphorylation loops, the network could start in one steady state, move to a second when the input pulse is turned on, but return to a different steady state when the pulse is turned off. Because we optimized for parameter values with zero network output before and after application of the input pulse, we implicitly selected for systems that do not exhibit bistability for the applied input. It would be interesting and should be feasible to select explicitly for bistable systems with this optimization technique.

Optimization has been applied here to search the parameterization landscape for a few different network topologies. This approach is complementary to direct parameter variation approaches, such as sensitivity analysis. Optimization is a useful framework to elucidate design principles in biological networks. The characteristics of an optimization landscape and resulting optimal solutions were examined for an enzymatic network element commonly found in signal transduction systems. While we have addressed relatively simple cases here, including the dynamic response to a single input rather than a family of inputs, for example, there are no conceptual barriers to applying the same approach to more complex cases. It will be interesting to see what, if any, changes to the optimal results occur in such computationally more challenging instances. Interestingly, the same network topology is capable of encoding multiple strategies depending on parameterization. Trade-offs exist when networks are required to achieve multiple goals, such as minimizing response-time while achieving a fixed amplitude. Elements of successful strategies for one network topology could be found in successful strategies for other networks. The availability of multiple strategies by changing rate constants but not connectivity may provide significant network performance gains through temporary rate modulation or evolution of more permanent rate changes.

Acknowledgements

We are grateful for discussions with Douglas A. Lauffenburger, Drew Endy, and members of our research groups, as well as for the comments of an anonymous referee. This work was partially supported by the National Institutes of Health (P50-GM68762).

References

1 T. Ideker, T. Galitski and L. Hood, A new approach to decoding life: systems biology, *Annu. Rev. Genomics Hum. Genet.*, 2001, **2**, 343–372.
2 H. S. Wiley, S. Y. Shvartsman and D. A. Lauffenburger, Computational modeling of the EGF-receptor system: a paradigm for systems biology, *Trends Cell Biol.*, 2003, **13**, 43–50.
3 A. Arkin, J. Ross and H. H. McAdams, Stochastic kinetic analysis of developmental pathway bifurcation, *Genetics*, 1998, **149**, 1633–1648.
4 C. V. Rao, J. R. Kirby and A. P. Arkin, Design and diversity in bacterial chemotaxis: a comparative study in *Escherichia coli* and *Bacillus subtilis*, *PLoS Biol.*, 2004, **2**, 239–252.
5 J. J. Tyson, Modeling the cell-division cycle Cdc2 and Cyclin interactions, *Proc. Natl. Acad. Sci. U. S. A.*, 1991, **88**, 7328–7332.

6 U. S. Bhalla and R. Iyengar, Emergent properties of networks of biological signaling pathways, *Science*, 1999, **283**, 381–387.
7 B. Schoeberl, C. Eichler-Jonsson, E. D. Gilles and G. Muller, Computational modeling of the dynamics of the MAP kinase cascade activated by surface and internalized EGF receptors, *Nat. Biotechnol.*, 2002, **20**, 370–375.
8 A. Hoffmann, A. Levchenko, M. L. Scott and D. Baltimore, The IκB-NF-κB signaling module: temporal control and selective gene activation, *Science*, 2002, **298**, 1241–1245.
9 A. R. Asthagiri and D. A. Lauffenburger, A computational study of feedback effects on signal dynamics in a mitogen-activated protein kinase (MAPK) pathway model, *Biotechnol. Prog.*, 2001, **17**, 227–239.
10 C. Y. Huang and J. E. Ferrell, Jr., Ultra-sensitivity in the mitogen-activated protein kinase cascade, *Proc. Natl. Acad. Sci. U. S. A.*, 1996, **93**, 10078–10083.
11 N. Barkai and S. Leibler, Robustness in simple biochemical networks, *Nature*, 1997, **387**, 913–917.
12 M. Thattai and A. van Oudenaarden, Intrinsic noise in gene regulatory networks, *Proc. Natl. Acad. Sci. U. S. A.*, 2001, **98**, 8614–8619.
13 D. Endy, D. Kong and J. Yin, Intracellular kinetics of a growing virus: a genetically structured simulation for bacteriophage T7, *Biotechnol. Bioeng.*, 1997, **55**, 375–389.
14 M. B. Elowitz, A. J. Levine, E. D. Siggia and P. S. Swain, Stochastic gene expression in a single cell, *Science*, 2002, **297**, 1183–1186.
15 T. Ideker, V. Thorsson, J. A. Ranish, R. Christmas, J. Buhler, J. K. Eng, R. Bumgarner, D. R. Goodlett, R. Aebersold and L. Hood, Integrated genomic and proteomic analyses of a systematically perturbed metabolic network, *Science*, 2001, **292**, 929–934.
16 A. R. Kansal and J. Trimmer, Application of predictive biosimulation within pharmaceutical clinical development: examples of significance for translational medicine and clinical trial design, *IEE Proc. Syst. Biol.*, 2005, **152**, 214–220.
17 A. K. Lewis, T. Paterson, C. C. Leong, N. Defranoux, S. T. Holgate and C. L. Stokes, The roles of cells and mediators in a computer model of chronic asthma, *Int. Arch. Allergy Immunol.*, 2001, **124**, 282–286.
18 R. Milo, S. Shen-Orr, S. Itzkovitz, N. Kashtan, D. Chklovskii and U. Alon, Network motifs: simple building blocks of complex networks, *Science*, 2002, **298**, 824–827.
19 E. H. Davidson, J. P. Rast, P. Oliveri, A. Ransick, C. Calestani, C. H. Yu, T. Minokawa, G. Amore, V. Hinman, C. Arenas-Mena, O. Otim, C. T. Brown, C. B. Livi, P. Y. Lee, R. Revilla, A. G. Rust, Z. Pan, M. J. Schilstra, P. J. Clarke, M. I. Arnone, L. Rowen, R. A. Cameron, D. R. McClay, L. Hood and H. Bolouri, A genomic regulatory network for development, *Science*, 2002, **295**, 1669–1678.
20 D. B. Forger and C. S. Peskin, A detailed predictive model of the mammalian circadian clock, *Proc. Natl. Acad. Sci. U. S. A.*, 2003, **100**, 14806–14811.
21 N. I. Markevich, J. B. Hoek and B. N. Kholodenko, Signaling switches and bistability arising from multisite phosphorylation in protein kinase cascades, *J. Cell Biol.*, 2004, **164**, 353–359.
22 R. J. Prill, P. A. Iglesias and A. Levchenko, Dynamic properties of network motifs contribute to biological network organization, *PLoS Biol.*, 2005, **3**, 1881–1892.
23 R. Heinrich, B. G. Neel and T. A. Rapoport, Mathematical models of protein kinase signal transduction, *Mol. Cell*, 2002, **9**, 957–970.
24 S. Chapman and A. R. Asthagiri, Resistance to signal activation governs design features of the MAP kinase signaling module, *Biotechnol. Bioeng.*, 2004, **85**, 311–322.
25 J. Stelling, E. D. Gilles and F. J. Doyle, III, Robustness properties of circadian clock architecture, *Proc. Natl. Acad. Sci. U. S. A.*, 2004, **101**, 13210–13215.
26 D. E. Zak, J. Stelling and F. J. Doyle, Sensitivity analysis of oscillatory (bio)chemical systems, *Comput. Chem. Eng.*, 2005, **29**, 663–673.
27 R. Gunawan, Y. Cao, L. Petzold and F. J. Doyle, Sensitivity analysis of discrete stochastic systems, *Biophys. J.*, 2005, **88**, 2530–2540.
28 M. S. Springer, M. F. Goy and J. Adler, Protein methylation in behavioural control mechanism and in signal transduction, *Nature*, 1979, **280**, 279–284.
29 A. Goldbeter, J. B. Stock and D. E. Koshland, Jr., Amplification and adaptation in regulatory and sensory systems, *Science*, 1982, **217**, 220–225.
30 D. T. Gillespie, Exact stochastic simulation of coupled chemical reactions, *J. Phys. Chem.*, 1977, **81**, 2340–2361.
31 W. F. Feehery, J. E. Tolsma and P. I. Barton, Efficient sensitivity analysis of large-scale differential-algebraic systems, *Appl. Numer. Math.*, 1997, **25**, 41–54.
32 J. E. Tolsma, J. A. Clabaugh and P. I. Barton, Symbolic incorporation of external procedures into process modeling environments, *Ind. Eng. Chem. Res.*, 2002, **41**, 3867–3876.
33 D. A. Schwer, J. E. Tolsma, W. H. Green, Jr. and P. I. Barton, On upgrading the numerics in combustion chemistry codes, *Combust. Flame*, 2002, **128**, 270–291.
34 I. S. Duff and J. K. Reid, A FORTRAN code for direct solution of sparse unsymmetric linear systems of equations, *Technical Report RAL-93-072*, Rutherford Appleton Laboratory, Oxon, UK, 1993.
35 K. E. Brenan, S. L. Campbell and L. R. Petzold, *Numerical Solution of Initial Value Problems in Differential-Algebraic Equations*, SIAM, Philadelphia, PA, 1996.
36 K. Teo, G. Goh and K. Wong, A Unified Computational Approach to Optimal Control Problems, *Pitman Monographs and Surveys in Pure and Applied Mathematics*, John Wiley and Sons, Inc., New York, 1991.
37 A. B. Singer and P. I. Barton, Global optimization with nonlinear ordinary differential equations, *J. Global Optim.*, 2006, **34**, 159–190.
38 P. E. Gill, W. Murray, M. A. Saunders and M. H. Wright, User's guide for NPSOL 5.0: A Fortran package for Nonlinear Programming, *Report SOL 86-1*, Department of Operations Research, Stanford University, Stanford, CA, 1998.
39 H. W. Kuhn and A. W. Tucker, Nonlinear programming, in *Proceedings of the Second Berkeley Symposium on Mathematical Statistics and Probability*, ed. J. Neyman, University of California Press, Berkeley, California, 1951.
40 M. S. Bazaraa, H. D. Sherali and C. M. Shetty, *Nonlinear Programming*, John Wiley and Sons, Inc., 2nd edn, 1993.
41 J. M. Smith, Optimization theory in evolution, *Annu. Rev. Ecol. Syst.*, 1978, **9**, 31–56.
42 S. A. Kauffman and E. D. Weinberger, The NK model of rugged fitness landscapes and its application to maturation of the immune response, *J. Theor. Biol.*, 1989, **141**, 211–245.
43 T. M. Yi, Y. Huang, M. I. Simon and J. Doyle, Robust perfect adaptation in bacterial chemotaxis through integral feedback control, *Proc. Natl. Acad. Sci. U. S. A.*, 2000, **97**, 46–49.
44 H. A. El-Masri and C. J. Portier, Replication potential of cells *via* the protein kinase C-MAPK pathway: application of a mathematical model, *Bull. Math. Biol.*, 1999, **61**, 379–398.